Multipulse Three-Dimensional Alignment of Asymmetric Top Molecules

Xiaoming Ren, Varun Makhija, and Vinod Kumarappan*
J. R. Macdonald Laboratory, Kansas State University, Manhattan, Kansas 66506, USA
(Received 20 June 2012; revised manuscript received 15 August 2013; published 30 April 2014)

We show, by computation and experiment, that a sequence of nonresonant and impulsive laser pulses with different ellipticities can effectively align asymmetric top molecules in three dimensions under field-free conditions. By solving the Schrödinger equation for the evolution of the rotational wave packet, we show that the 3D alignment of 3,5 difluoroiodobenzene molecules improves with each successive pulse. Experimentally, a sequence of three pulses is used to demonstrate these results, which extend the multipulse schemes used for 1D alignment to full 3D control of rotational motion.

DOI: 10.1103/PhysRevLett.112.173602 PACS numbers: 42.50.Hz, 33.15.Bh, 33.80.-b, 37.10.Vz

The development of molecular alignment techniques—which force the axes of gas-phase molecules to line up with laboratory axes and enable measurements in the molecular frame—such as hexapole focusing [1], brute-force orientation [2,3], and intense laser alignment [4–7] has enabled investigations of a variety of phenomena including stereochemistry [1,8], gas-phase x-ray [9,10] and electron diffraction [11–13], strong-field photoionization [14,15], and high-harmonic generation in molecules [16]. The vast majority of such experiments have been carried out in linear or symmetric top molecules, or asymmetric tops aligned only in one dimension, due to the difficulty of aligning and orienting asymmetric tops in all three dimensions. In order to perform molecular frame measurements with asymmetric tops, experimental techniques to overcome these difficulties need to be developed. It is also often necessary to align or orient molecules under field-free conditions to avoid the detrimental influence of strong external fields on the process being studied. In this Letter we demonstrate, through computational and experimental means, a significant advance in field-free 3D alignment (FF3DA) of asymmetric tops: we show that a nonresonant multipulse excitation scheme can progressively improve the alignment of all three axes of an asymmetric top, leading to strong FF3DA.

The interaction of the molecular polarizability with an intense nonresonant laser pulse can be used to align molecular axes with laser polarization axes [5]. Using this interaction, three-dimensional alignment (3DA) of molecules was first obtained within a long elliptically polarized laser pulse [17]. When using cold or state-selected molecules, the adiabatic scheme can produce excellent one-dimensional alignment (1DA) [18,19] and good 3DA [20], which can be further improved by using a short pulse in the "hold and spin" scheme [21]. Two orthogonally polarized and time-separated short pulses can produce FF3DA [22,23]. This scheme involves aligning one axis of the molecule, and then trying to spin it around this axis. The first axis alignment is inevitably perturbed by the second pulse, limiting the strength and duration of FF3DA. Elliptically polarized short pulses have also been shown to generate FF3DA [24,25], although a sequence of identical elliptical pulses was shown not to be effective for SO_2 [26]. In this Letter, we show, using 3,5 difluoroiodobenzene (DFIB) as an example, that FF3DA of an asymmetric top with prolate-type inertia and polarizability tensors can be progressively improved by a sequence of elliptical pulses following a linear pulse. The linear pulse aligns the C-I axis and the subsequent elliptical pulses align all three axes simultaneously. The basis for choosing the proposed sequence of pulses will be discussed, followed by a demonstration of the effectiveness of the scheme from the nonperturbative solution of the rigid-rotor time-dependent Schrödinger equation (TDSE) for DFIB for a sequence of four pulses. We will also show experimental evidence from velocity map imaging (VMI) of I^+ and F^+ ions after a three-pulse sequence that the suggested scheme does produce substantial FF3DA. Our results show that multipulse methods developed for FF1DA [27–31] can indeed be adapted to FF3DA, provided pulses of different ellipticities are used. This is in contrast with Ref. [26], where a train of identical elliptical pulses was considered and shown not to be effective.

The TDSE for a rigid asymmetric top rotor in the ground vibronic state interacting with an intense nonresonant pulse not strong enough to excite vibronic transitions out of the ground state has been discussed several times (see Ref. [32] for a review), and we will not delve into the details. Briefly, the rotor wave function is expressed in the symmetric top basis for in-field evolution, and then converted to the asymmetric top basis for field-free propagation. A thermal distribution (at 1K) of rotational states weighted by nuclear spin statistics was used [33].

The degree of 3DA is determined by calculating $\langle \cos^2\delta \rangle$, a measure proposed in Ref. [34]. Briefly, since 3DA has D_2 symmetry, there are four equivalent target orientations. In the axis-angle representation, the squared cosines of the angles of the rotations that take an arbitrarily oriented

molecule to these four targets are averaged to construct $\langle\cos^2\delta\rangle$, which is 1 for perfect alignment of all three axes, 1/2 for an isotropic distribution and 3/4 if any one axis is perfectly aligned and the other two are randomly distributed. In order to examine the alignment of individual axes, we also calculate the evolution of $\langle\cos^2\theta_{mL}\rangle$, where m stands for the three principal axes of the moments of inertia ($m = a, b, c$. See Fig. 1) of the molecules, L denotes the laboratory frame axes XYZ, with Z defined as the polarization axis of the first (linearly polarized) laser pulse, X as the minor polarization axes of the subsequent elliptical pulses, and Y as the propagation axes of all pulses. θ_{mL} is the corresponding enclosed angle.

The first pulse is linearly polarized in order to pick out the favored laboratory axis for the most polarizable molecular axis, since this axis is most easily aligned when the polarizability tensor is of the prolate type. Then, each elliptical pulse is timed to occur just before the peak 3DA induced by the previous pulses, with the precise timing determined largely by trial and error. The number of pulses is limited because the alignment peaks faster after each successive pulse, limiting the time available for an additional pulse. The choice of ellipticity depends on the molecule; however, a general trend can be determined by comparing the matrix elements of $\cos^2\delta$ and the interaction Hamiltonian. These can be written analytically in the symmetric top basis $|JKM\rangle$, where J is the total angular momentum and K and M are the projections along the molecular symmetry axis and the Z axis, respectively. The laser electric field has the form

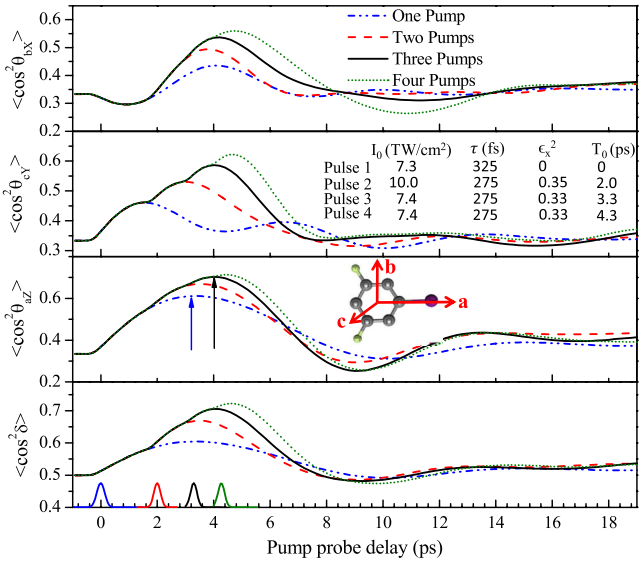

FIG. 1 (color online). Time evolution of $\langle\cos^2\theta_{bX,cY,aZ}\rangle$ and $\langle\cos^2\delta\rangle$ after a sequence of pulses. Pump pulse parameters (peak intensity I_0, pulse width τ, ellipticity parameter ϵ_X^2 and delays T_0) are listed in the table, and the pulses are shown on the delay axis. The molecular frame axes are also shown. For DFIB, $\alpha_{aa} = 21.5$ Å^3, $\alpha_{bb} = 15.3$ Å^3, $\alpha_{cc} = 10.2$ Å^3, and $A = 1.74$ GHz, $B = 0.484$ GHz, and $C = 0.379$ GHz [35].

$\mathbf{E}(t) = E_0(t)[\epsilon_X\cos(\omega t)\mathbf{e}_X + \epsilon_Z\sin(\omega t)\mathbf{e}_Z]$, where ω is the frequency and ϵ_X and ϵ_Z are the relative weights of the amplitudes of the X and Z components, respectively (with $\epsilon_X^2 + \epsilon_Z^2 = 1$). The matrix elements are [9,34]

$$\langle JKM|H_I(t)|J'K'M'\rangle = 4\pi\alpha I(t)\left[\frac{(2-3\epsilon_X^2)}{\sqrt{6}}\langle JM;2,0|J'M'\rangle + \frac{\epsilon_X^2}{2}(\langle JM;2,2|J'M'\rangle + \langle JM;2,-2|J'M'\rangle)\right] \times\left[\alpha_0^2\langle JK;2,0|J'K'\rangle + \alpha_2^2(\langle JK;2,2|J'K'\rangle + \langle JK;2,-2|J'K'\rangle)\right], \quad (1)$$

$$\langle JKM|\cos^2\delta|J'K'M'\rangle = \frac{1}{4} + \frac{1}{4}\delta_{JJ'}\delta_{KK'}\delta_{MM'} + \frac{1}{4}\sqrt{\frac{2J+1}{2J'+1}}\langle J,M;2,0|J',M'\rangle\langle J,K;2,0|J',K'\rangle + \frac{1}{8}\sqrt{\frac{2J+1}{2J'+1}}\{[\langle J,K;2,2|J',K'\rangle + \langle J,K;2,-2|J',K'\rangle][\langle J,M;2,2|J',M'\rangle + \langle J,M;2,-2|J',M'\rangle]\}, \quad (2)$$

where $I(t)$ is the time-dependent intensity of the pulse in atomic units, α is the fine structure constant, α_m^l are spherical components of the molecular polarizability tensor and $\langle J,M;J',M'|J'',M''\rangle$ are the Clebsch-Gordan coefficients. The coherences excited by this interaction must be viewed in terms of the goal of the experiment—maximizing the value of $\langle\cos^2\delta\rangle$. We label the product terms by ΔK and ΔM: the term with $\Delta K, M = 0$ is called the 00 term, the term with $\Delta K = 0$ and $\Delta M = \pm 2$ is called the 02 term and so on. $\langle\cos^2\delta\rangle$ has contributions from 00 and 22 terms, but not from 02 and 20 terms. The 00 term measures the 1D alignment of the a axis and the 22 term the simultaneous alignment of the b and c axes [34]. All four terms appear in H_I and there is an additional $\Delta K = \pm 2$, $\Delta M = 0$ contribution in the total Hamiltonian from the field-free asymmetric top Hamiltonian, which conserves M but not K [36]. We must, therefore, choose a value of $\mathbf{e}_X^2$ that provides a substantial contribution to 00 and 22 terms [37]. Also, since the 00 and 22 coherences can each contribute up to 1/4 to $\langle\cos^2\delta\rangle$, it is imperative not to

compromise substantially on the former (i.e., 1DA) to boost the latter.

Our solution to this problem is to use multiple pulses of different ellipticities, an extension of the two-pulse method [22,23]. In this manner, not only can different terms in Eq. (2) be emphasized by different pulses, the timing of the pulses can be tailored to the different time scales of the molecular axes. We show that a sequence of elliptical pulses following a linear pulse can be used effectively in this manner for a molecule with a prolate-type polarizability tensor. The linearly polarized first pulse ($\epsilon_X = 0$) aligns the a axis through the 00 term in Eq. (1). If the following elliptical pulse has $\epsilon_X^2 > 2/3$, this term becomes negative and degrades the 1DA induced by the first pulse and, therefore, has a detrimental effect on 3DA too. However, if $\epsilon_X^2 \leq 2/3$, the second pulse can align all three axes through the 00 and 22 terms. Therefore, for this scheme to be effective ϵ_X^2 must be less than $2/3$ for all the elliptical pulses. In order to excite a broad wave packet in K and M and to synchronize the peaks in the alignment of individual axes, multiple elliptical pulses—each below the ionization threshold—are used.

In Fig. 1 we show the evolution of $\langle \cos^2\theta_{bX,cY,aZ} \rangle$ and $\langle \cos^2\delta \rangle$ after sequences of up to four pulses. Intensities and durations for the first three pulses are those we are limited to by experimental constraints. The ellipticities were chosen by starting with $\epsilon_X^2 = 2/3$, and systematically reducing them to increase $\langle \cos^2\delta \rangle$. Each pulse after the first one arrives a few hundred fs before the peak of $\langle \cos^2\delta \rangle$ due to all the previous pulses. Even though some of these choices are determined by experimental considerations rather than the optimization of FF3DA, it is clear from the results of the TDSE calculation that this scheme does lead to an improvement in the alignment of all three axes after each pulse. In particular, the alignment of the a axis is improved rather that degraded by subsequent pulses and the peak alignment of each axis occurs at approximately the same time.

In the experiment, DFIB molecules were seeded in a pulsed high-pressure helium jet [38] and rotationally cooled to ~1 K [18]. Pulses from a 2 mJ/pulse, 30 fs, 2 kHz Ti:sapphire laser were split into four beams using low-dispersion beam splitters. The beams were recombined and overlapped in space and time and focused into a VMI spectrometer in a vacuum chamber. Two of the three pump pulses were delayed by manual delay stages while the probe beam, which multiply ionized and fragmented the molecules, was delayed by a computer-controlled stage. The polarizations were controlled using zero-order half- and quarter-wave plates. The pumps were weak enough to produce negligible fragmentation; this was confirmed by measuring the ion time-of-flight spectrum without the probe pulse. The I^+ and F^+ ions were selected by applying high-voltage gates to the front of the microchannel plate detector in the spectrometer, and imaged with a high-speed camera.

Figure 2 shows measured 2D momentum distributions of I^+ and F^+ ions for several polarization configurations at delays where maximum alignment is achieved by the

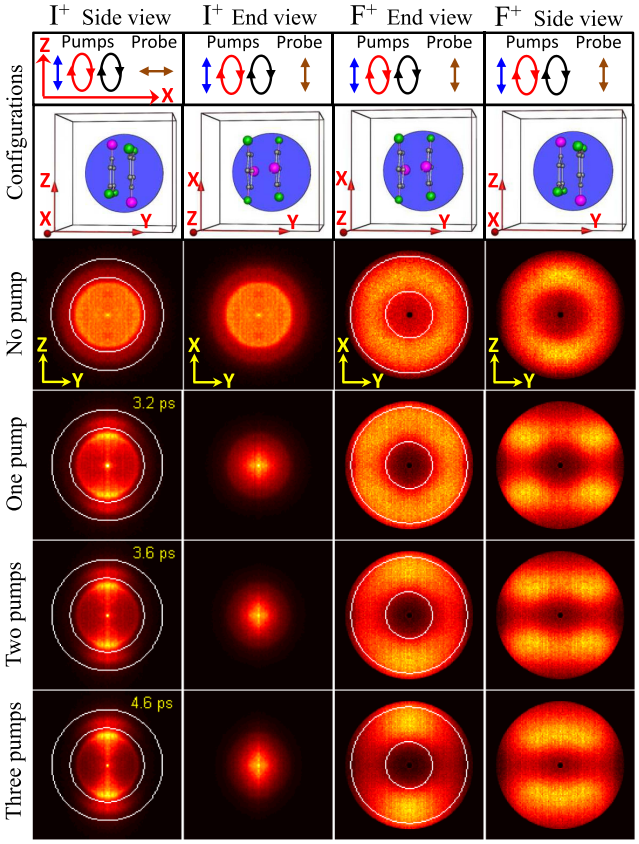

FIG. 2 (color online). Velocity maps of I^+ and F^+ ions from unaligned molecules and at peak alignment after each pump pulse. The top two rows show the polarizations of the pumps and probe relative to the VMI detector (blue disc) for each column beneath. The XYZ axes and the desired orientation of the molecules is also shown. Note that the pump pulses, rather than the physical laboratory, define the "laboratory frame" axes XYZ for practical reasons: it is much easier to rotate the molecules (by rotating the polarizations of all the pump pulses) and keep the spectrometer fixed for measuring the different projections. Circles mark annular regions over which $\langle \cos^2\theta_{2D} \rangle$ is calculated; the evolution of these is shown in Fig. 3.

preceding pulses. We define "end" and "side" views of both fragments based on the direction of alignment of the a axis [21]: if this axis is parallel (perpendicular) to the plane of the detector, the projection of the momentum distribution is called a side (end) view. VMI of fragment ions from a 3D-aligned ensemble requires careful consideration of alignment axes and probe polarization vectors because of the sensitivity of the Coulomb explosion process to the polarization of the probe pulse and due to the impossibility of retrieving the full fragment momentum distribution from a single projection. The probe was polarized perpendicular to the detector for the first three columns and along the Z axis for the last one in an attempt to minimize these complications, and in an effort to distinguish between confinement of the a axis to the XZ plane and its confinement to the Z axis. This distinction is particularly difficult to make in the side view of I^+ fragments, unless this axis is

very strongly aligned [21]. The side and end view images of I^+ and F^+ ions are shown without any pumps to characterize probe bias and at peak alignment after each pump pulse. End view images of I^+ show that the a axis remains aligned with the Z axis. In order to quantify the degree of alignment obtained, we measure $\langle\cos^2\theta_{2D}\rangle$, where θ_{2D} is the angle between projections of the ion velocity vector and laser polarization plane on the detector (see Fig. 2). In Fig. 3, we show the time evolution of $\langle\cos^2\theta_{2D}\rangle$ for I^+ (side view) and F^+ (end view) ions calculated in the annular regions marked in Fig. 2. The former measures the alignment of the a axis, and the latter that of the molecular plane given that the a axis is aligned perpendicular to the plane. As expected, the linearly polarized first pump aligns only the a axis, after which both elliptical pumps improve the alignment of the a axis and align the molecular plane, simultaneously.

For better characterization of FF3DA and to distinguish between confinement of the a axis to the XZ plane and its confinement to the Z axis, we measure the full 3D momentum distribution of the I^+ ions by combining VMI and tomography in momentum space [39]. In order to implement this technique in our setup, we rotate the polarizations of all our beams simultaneously using an achromatic zero-order half-wave plate after all the beams have been recombined. In this case we use a circular probe, since the greatest ambiguity in our VMI spectra is the nature of the localization of the I^+ ion in the polarization plane. We measure 90 projections with a step size of 2°, and use a filtered back-projection algorithm [40] for the reconstruction of the 3D momentum distribution. Figure 4 shows isosurface plots of the I^+ momentum distribution at the peak of 1DA after the first pump, and of 3DA after the third pump. These plots show that the a axis remains well aligned with the Z axis rather than getting redistributed to the XZ plane after the elliptical pump pulses. The disappearance of the dark red region near $V_Z \approx 0$ shows that poorly aligned molecules have been swept towards the Z axis by the elliptical pulses. These pulses also make the distribution in the V_XV_Z plane somewhat broader than that in the V_ZV_Y plane due to the action of the minor axis of the elliptical field, which is along the X axis. When combined with the fluorine projections shown in Fig. 2, these images show FF3DA unambiguously. Furthermore, from the 3D distributions we get $\langle\cos^2\theta_{aZ}\rangle = 0.56$ and 0.65 for FF1DA and FF3DA, respectively. The calculated values shown in Fig. 1 are 0.61 and 0.70 (indicated by the arrows). Note that the calculations do not account for probe selectivity and volume averaging effects and, in the absence of coincidence information, it was also not possible to measure $\langle\cos^2\delta\rangle$. For these reasons a direct quantitative comparison was not intended, but the measurements show good qualitative agreement with the calculations and confirm the main features of the proposed scheme. The calculated maximum of $\langle\cos^2\delta\rangle$ after three pulses is 0.71. For comparison, Lee *et al.* [23] and Rouzee *et al.* [24] achieve $\langle\cos^2\delta\rangle = 0.63$ (in this case, 1D alignment by the first pulse already produces $\langle\cos^2\delta\rangle = 0.62$) and 0.52, respectively, as calculated from their experimental parameters. Our scheme also permits further enhancement in the alignment with the addition of more pulses.

While our demonstration of a scheme for progressively improving FF3DA in asymmetric top molecules is an important step forward, it is clear that multipulse FF3DA has a very large parameter space in terms of laser intensities, ellipticities, pulse durations, and delays. The pulse sequences used here were picked due to a combination of physical motivation and practical constraints, but the complexity of the problem means that these choices are very likely not the best ones. We have checked that the combination of a linearly polarized pulse and a sequence of elliptical pulses is effective for other asymmetric tops with a prolatelike polarizability, but not for those with oblatelike polarizability. In the latter case, making the first pulse elliptical is a better choice because it is easier to confine the least polarizable axis to the laser propagation direction

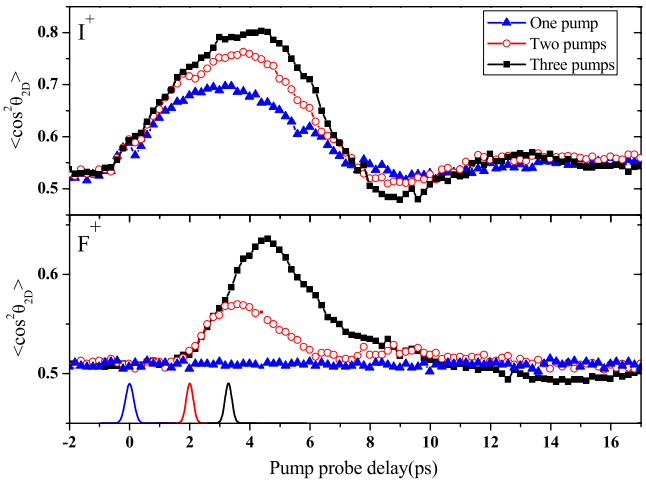

FIG. 3 (color online). Evolution of $\langle\cos^2\theta_{2D}\rangle$ for I^+ and F^+ ions. The laser pulse parameters are given in Fig. 1; only the first three pulses were used.

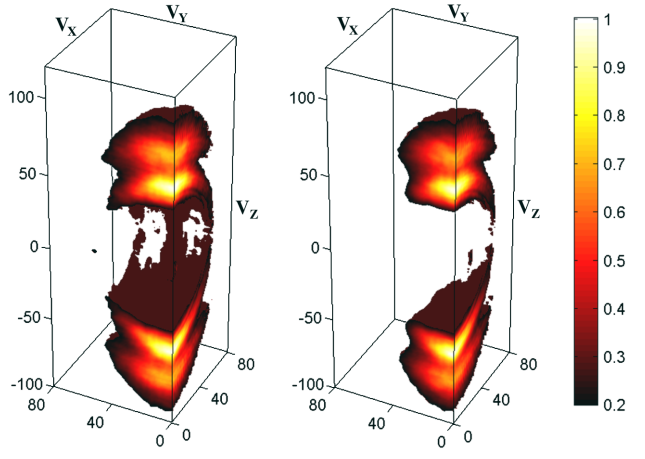

FIG. 4 (color online). 3D velocity distributions of I^+, at the peaks of 1D (left, at 3.2 ps) and 3D (right, at 4.6 ps) alignment. The distributions were normalized to the peak values, and the velocities are in arbitrary units.

rather than aligning the most-polarizable axis with the Z axis. The details of these calculations will be reported elsewhere. An interesting option would be to use a polarization pulse shaper [41] with a feedback optimization loop involving, for instance, a genetic algorithm for searching the parameter space. Computationally, an optimal control algorithm could be used for the same purpose; Ref. [25] addressed this issue with the search space restricted to two orthogonally polarized pulses that could be combined into one elliptical pulse.

Since the first demonstration of 3DA [17], it has been clear that good FF3DA will enable many novel experiments, greatly expanding the already widely used 1DA of molecules. With our experimental and theoretical results, we have shown that a multipulse scheme tailored to the properties of the molecules can produce substantial FF3DA. kHz repetition rate lasers with sufficient energy output to both align the molecules and do subsequent measurements are increasingly common and we expect that our technique will enable new molecular-frame measurements on asymmetric tops in strong-field physics, molecular imaging, and photoelectron spectroscopy, among others.

This work was supported by the Chemical Sciences, Geosciences, and Biosciences Division, Office of Basic Energy Sciences, Office of Science, U.S. Department of Energy. The computing for this project was performed on Beocat, the campus research computing cluster at Kansas State University, which is funded in part by NSF Grants No. CNS-1006860, No. EPS-1006860, and No. EPS-0919443.

*vinod@phys.ksu.edu

[1] P. R. Brooks and E. M. Jones, J. Chem. Phys. **45**, 3449 (1966).
[2] H. J. Loesch and A. Remscheid, J. Chem. Phys. **93**, 4779 (1990).
[3] B. Friedrich and D. Herschbach, Nature (London) **353**, 412 (1991).
[4] D. Normand, L. A. Lompre, and C. Cornaggia, J. Phys. B **25**, L497 (1992).
[5] B. Friedrich and D. Herschbach, Phys. Rev. Lett. **74**, 4623 (1995).
[6] T. Seideman, Phys. Rev. Lett. **83**, 4971 (1999).
[7] F. Rosca-Pruna and M. J. J. Vrakking, Phys. Rev. Lett. **87**, 153902 (2001).
[8] D. H. Parker and R. B. Bernstein, Annu. Rev. Phys. Chem. **40**, 561 (1989).
[9] S. Pabst, P. J. Ho, and R. Santra, Phys. Rev. A **81**, 043425 (2010).
[10] J. Küpper *et al.*, Phys. Rev. Lett. **112**, 083002 (2014).
[11] M. Meckel, D. Comtois, D. Zeidler, A. Staudte, D. Pavičić, H. C. Bandulet, H. Pépin, J. C. Kieffer, R. Dörner, D. M. Villeneuve, and P. B. Corkum, Science **320**, 1478 (2008).
[12] P. Reckenthaeler, M. Centurion, W. Fuß, S. A. Trushin, F. Krausz, and E. E. Fill, Phys. Rev. Lett. **102**, 213001 (2009).
[13] C. J. Hensley, J. Yang, and M. Centurion, Phys. Rev. Lett. **109**, 133202 (2012).
[14] V. Kumarappan, L. Holmegaard, C. Martiny, C. B. Madsen, T. K. Kjeldsen, S. S. Viftrup, L. B. Madsen, and H. Stapelfeldt, Phys. Rev. Lett. **100**, 093006 (2008).
[15] L. Holmegaard *et al.*, Nat. Phys. **6**, 428 (2010).
[16] R. Velotta, N. Hay, M. B. Mason, M. Castillejo, and J. P. Marangos, Phys. Rev. Lett. **87**, 183901 (2001).
[17] J. J. Larsen, K. Hald, N. Bjerre, H. Stapelfeldt, and T. Seideman, Phys. Rev. Lett. **85**, 2470 (2000).
[18] V. Kumarappan, C. Z. Bisgaard, S. S. Viftrup, L. Holmegaard, and H. Stapelfeldt, J. Chem. Phys. **125**, 194309 (2006).
[19] L. Holmegaard, J. H. Nielsen, I. Nevo, H. Stapelfeldt, F. Filsinger, J. Kupper, and G. Meijer, Phys. Rev. Lett. **102**, 023001 (2009).
[20] I. Nevo, L. Holmegaard, J. H. Nielsen, J. L. Hansen, H. Stapelfeldt, G. Filsinger, F. Meijer, and J. Kupper, Phys. Chem. Chem. Phys. **11**, 9912 (2009).
[21] S. S. Viftrup, V. Kumarappan, S. Trippel, H. Stapelfeldt, E. Hamilton, and T. Seideman, Phys. Rev. Lett. **99**, 143602 (2007).
[22] J. G. Underwood, B. J. Sussman, and A. Stolow, Phys. Rev. Lett. **94**, 143002 (2005).
[23] K. F. Lee, D. M. Villeneuve, P. B. Corkum, A. Stolow, and J. G. Underwood, Phys. Rev. Lett. **97**, 173001 (2006).
[24] A. Rouzée, S. Guérin, O. Faucher, and B. Lavorel, Phys. Rev. A **77**, 043412 (2008).
[25] M. Artamonov and T. Seideman, Phys. Rev. A **82**, 023413 (2010).
[26] S. Pabst and R. Santra, Phys. Rev. A **81**, 065401 (2010).
[27] I. S. Averbukh and R. Arvieu, Phys. Rev. Lett. **87**, 163601 (2001).
[28] M. Leibscher, I. S. Averbukh, and H. Rabitz, Phys. Rev. Lett. **90**, 213001 (2003).
[29] K. F. Lee, I. V. Litvinyuk, P. W. Dooley, M. Spanner, D. M. Villeneuve, and P. B. Corkum, J. Phys. B **37**, L43 (2004).
[30] C. Z. Bisgaard, M. D. Poulsen, E. Péronne, S. S. Viftrup, and H. Stapelfeldt, Phys. Rev. Lett. **92**, 173004 (2004).
[31] J. P. Cryan, P. H. Bucksbaum, and R. N. Coffee, Phys. Rev. A **80**, 063412 (2009).
[32] M. Artamonov and T. Seideman, J. Chem. Phys. **128**, 154313 (2008).
[33] Nuclear spin weights for rotational states with A, B_a, B_b, and B_c symmetry [36] are 10, 10, 6, and 6, respectively.
[34] V. Makhija, X. Ren, and V. Kumarappan, Phys. Rev. A **85**, 033425 (2012).
[35] S. S. Viftrup, V. Kumarappan, L. Holmegaard, C. Z. Bisgaard, H. Stapelfeldt, M. Artamonov, E. Hamilton, and T. Seideman, Phys. Rev. A **79**, 023404 (2009).
[36] R. N. Zare, *Angular Momentum: Understanding Spatial Aspects in Chemistry and Physics* (Wiley-Interscience, New York, 1988).
[37] The role of the 20 and 02 terms is less clear, although artificially removing them from H_I improves 3DA in our simulations.
[38] U. Even, J. Jortner, D. Noy, N. Lavie, and C. Cossart-Magos, J. Chem. Phys. **112**, 8068 (2000).
[39] M. Wollenhaupt, M. Krug, J. Köhler, T. Bayer, C. Sarpe-Tudoran, and T. Baumert, Appl. Phys. B **95**, 647 (2009).
[40] G. T. Herman, *Fundamentals of Computerized Tomography: Image Reconstruction from Projections, Adv. Pattern Recognition* (Springer, London, 2009).
[41] T. Brixner and G. Gerber, Opt. Lett. **26**, 557 (2001).